Available online at www.sciencedirect.com
ScienceDirect
Trans. Nonferrous Met. Soc. China 35(2025) 1017−1031
Transactions of Nonferrous Metals Society of China
www.tnmsc.cn

Engineering heterogeneous microstructures for enhanced strength and ductility in air-cooled Al−Mg−Si alloys

Yi-han GAO[1], Xin-xin ZHANG[2], Jing-zhe ZHOU[3], Peng XU[1], Zhi-jie XIN[4], Jun-hua GAO[4], Yan-hao SHI[4], You LÜ[2], Yu-fang ZHAO[4], Jing-yang LI[1]

1. School of Aerospace Engineering, North University of China, Taiyuan 030051, China;
2. Key Laboratory of Material Chemistry for Energy Conversion and Storage, Ministry of Education, Hubei Key Laboratory of Material Chemistry and Service Failure, School of Chemistry and Chemical Engineering, Huazhong University of Science and Technology, Wuhan 430074, China;
3. R&D Material Division, Press Metal International Ltd., Foshan 528137, China;
4. School of Mechanical Engineering, North University of China, Taiyuan 030051, China

Received 17 August 2023; accepted 21 June 2024

Abstract: The heterogeneity of α-Al(Fe,Mn)Si dispersoids and β'' precipitates was tuned to enhance the strength−ductility synergy of air-cooled Al−Mg−Si alloys. Scanning electron microscopy (SEM) and transmission electron microscopy (TEM) were employed to elucidate the microstructural parameters of these two strengthening phases. The results show that the microstructural heterogeneity can be triggered by the absence of homogenization, resulting in the presence of dispersoid-free zones (DFZs) and dispersoid zones (DZs), in conjunction with bimodal β'' precipitates. Further analytical calculations, from the strengthening model, clarify that the strategically dispersed α-Al(Fe,Mn)Si and β'' particles create "soft" and "hard" domains within the alloy, resultantly improving the mechanical properties.
Key words: Al−Mg−Si alloy; microstructure heterogeneity; dispersoid; nanoprecipitate; mechanical property

1 Introduction

6xxx series (Al−Mg−Si-based) alloys are highly favourable for the fabrication of structural components in the transportation industry due to their desirable mechanical properties, formability, weldability and corrosion resistance [1−3]. Over the past century, commercial 6xxx alloys such as 6082 [4], 6005A [5] and 6061 [6] have been developed for fabricating hollow profiles with complex sections and resultantly high structure stiffness. As a result, these alloys receive increasing attentions from researchers in the fields of automotive, navy and consumer electronics. However, it is worth noting that one of the most well-known disadvantages of 6xxx alloys is the moderate strength. For instance, the tensile strength of Al−Mg−Si alloys is usually <400 MPa [7], which is not as high as their competitors such as 2xxx (Al−Cu-based) [8,9] and 7xxx (Al−Zn−Mg−Cu-based [10,11]) alloys. In response to this limitation, numerous attempts have been made to enhance the age-hardening effects by assembling multiple contributors including nanoprecipitates, dispersoids, grain boundaries and forest dislocations. The corresponding techniques, such as microalloying [12,13] and severe plastic deformation (SPD) [14],

Corresponding author: Yi-han GAO, Tel: +86-351-3922615, E-mail: yhgao@nuc.edu.cn;
Xin-xin ZHANG, Tel: +86-27-87543032, E-mail: xinxinzhang@hust.edu.cn;
Yu-fang ZHAO, Tel: +86-351-3925466, E-mail: yufangzhao@nuc.edu.cn
DOI: https://doi.org/10.1016/S1003-6326(24)66731-2

have been well developed by many pioneers in past decades, constantly approaching to strengthen Al−Mg−Si alloys.

Generally speaking, the thermomechanical treatment plays an essential role in tailoring the mechanical properties of Al-based alloys by manipulating their microstructure. For the 6xxx Al profiles, the traditional thermomechanical process usually includes homogenization, hot extrusion, quenching and the final artificial aging [15,16]. Among these steps, homogenization at high temperature serves as a necessary precursor step enabling enhanced formability during subsequent extrusion processes. The choice for higher homogenization temperatures has been extensively reported in many commercial 6xxx alloys [17,18]. One reason for this choice is to eliminate solute segregation by thermally activating solute diffusion [3]. Additionally, thermal exposure at such temperatures allows the dissolution and/or phase transformation of brittle eutectic phases and constituents, including α-AlFeSi, Q-$Al_4Cu_2Mg_8Si_7$ and β-Mg_2Si phases in Al−Mg−Si alloys [19−21]. Furthermore, dispersoids are representatively observed during homogenization at such temperature, such as α-Al(Fe,Mn)Si dispersoids in the studied 6082 alloy. It is worth noting that forming dispersoids has dual effects in Al−Mg−Si alloys.

On the one hand, α-Al(Fe,Mn)Si dispersoids with characteristic sizes ranging from tens of nanometres to over 100 nanometres are helpful to strengthen the alloy and, importantly, suppress recrystallization during high-temperature extrusion by pining grain boundaries [5,17,22,23]. On the other hand, if Si solutes are greatly consumed by α-Al(Fe,Mn)Si particles, then the formation of (Mg,Si)-rich nanoprecipitates strengthening will be correspondingly weakened. For example, a recent work proposed by WANG et al [19] shows that the solute competition between α-Al(Fe,Mn)Si dispersoids and (Mg,Si)-rich nanoprecipitates is effectively tailored by homogenization, which plays a key role in the age-hardening response. By the way, quenching process is also another crucial step applied after homogenization and extrusion for commercial Al−Mg−Si alloys to heavily affect the mechanical properties [24]. A series of recent reports further suggested that quenching procedures tailor the starting vacancy site fractions before aging, thus controlling the precipitation nucleating on solute clusters forming at a very early stage of aging [1].

Theoretically, sufficient homogenization and rapid cooling rate (like water quenching) are favourable in 6xxx Al alloys for achieving optimal mechanical properties [7,15,19]. In this term, high supersaturation of solutes/vacancies and fully suppressed quench-in precipitation are acquired, leading to the formation of dense (Mg,Si)-rich nanoprecipitates during subsequent artificial aging. However, a large number of 6xxx series alloys have to tolerate the insufficient homogenization duration and low quenching rate. Two main reasons are given below. Firstly, the fabrication of these extruded alloys is expected to skip the homogenization step and be directly hot extruded from the as-cast state to save the cost [19]. Secondly, the cooling rate must be strictly limited in the component with a complex cross section (varying wall dimensions and hollows) to guarantee the high structural accuracy. In such cases, the procedure of water quenching has to be replaced by spray quenching or, usually, air cooling, aiming to achieve uniform cooling rate and prevent residual stress/distortion, even at the expense of the alloying elements consumption by coarse intermetallics to jeopardize strength [25].

Although the individual effect of homogenization and quenching procedure have been well-studied, a scientific question still remains: is it possible to utilize the microstructural heterogeneity in Al−Mg−Si alloys equipped with dual strengthening phases of dispersoids and nanoprecipitates? In fact, the heterogeneous dispersion of dispersoids is universally observed in the Mn-containing alloys such as commercial 3xxx [22,26] and 6xxx series [27]. This mainly originates from the positive solid–liquid partition coefficient k_0 (~0.7) of Mn [28], resulting in the Mn depletion in the interdendritic regions during solidification and presenting as the microstructural defect of dispersoid free zones (DFZs) in extruded alloys. Unfortunately, such heterogeneity is often negative and should be eliminated by performing homogenization [19]. However, in this work, some clues that the heterogeneous α-Al(Fe,Mn)Si dispersoids and β'' nanoprecipitates can be synergistically triggered in an air-cooled 6082 alloy, are present. Most importantly, such heterogeneity can be utilized to improve the mechanical properties.

2 Experimental

2.1 Sample preparation

A 6082 extruded alloy with nominal composition given in Table 1 was used in the study. The profiles with symmetrical four hollows were prepared with uniform wall thickness of ~2 mm, extrusion ratio of ~37 and extrusion speed of ~2 mm/s. Two typical abbreviations used in this work, denoted as the 6082-H and 6082-U, are distinguished by performing the homogenization or not before the extrusion (H−Homogenized, U−Unhomogenized). In detail, the 6082-U alloy has a simplified thermomechanical process of being melted, cast, hot-extruded, air-cooled and artificially aged at 185 °C for 5 h. In contrast, the 6082-H alloy has an extra homogenization protocol at 480 °C for 4 h after casting and before extrusion to complete the traditional thermomechanical procedure. Noted that the temperature of the alloys exiting the extrusion mould is detected as (500±2) °C before quenching, and the duration of room-temperature storage between quenching and artificial aging is strictly controlled as 24 h in all studied alloys. Moreover, different quenchants were also utilized for comparative experiments, including air-cooled (AC) and water-quenching (WQ).

Table 1 Composition of studied 6082 alloy (wt.%)

Si	Mg	Mn	Fe	Cu	Cr	Ti	Zn	Al
1.02	0.76	0.54	0.20	0.01	0.05	0.03	0.05	Bal.

2.2 Mechanical property tests

The room-temperature tensile tests were performed to evaluate the mechanical properties of studied alloys, using dog-bone shaped samples with a gauge dimension of 25 mm in length, 6 mm in width and 2 mm in thickness. An extensometer was employed to record the strain, and at least 5 samples were tested to generate the representative tensile curves. The tensile direction is parallel with the extrusion direction.

2.3 Microstructural characterization

The studied alloys were characterized by scanning electron microscopy (SEM), electron backscatter diffraction (EBSD), transmission electron microscopy (TEM), high resolution TEM (HRTEM), atomic-resolution high-angle annular dark-field scanning transmission electron microscopy (HAADF-STEM) and energy disperse spectroscopy (EDS). The SEM and EBSD specimens were mechanically ground and polished by 1 μm diamond paste to acquire the mirror surfaces. Subsequently, electropolishing was performed in a mixture of 700 mL ethanol and 300 mL perchloric acid at ~7 °C. Finally, the specimens were ultrasonically cleaned in an acetone bath and dried using cool air flow. TEM foils were prepared through twin-jet electropolishing using a solution of 80 vol.% methanol and 20 vol.% nitric acid at temperature of ~−30 °C and a voltage of ~20 V. Noted that the microstructural parameters of second-phase particles, such as radius r, number density N_v and volume fraction f_v, were quantitatively measured following the methods proposed in Refs. [29,30]. For simplicity purposes, further details can be found in our previous work [31,32].

3 Results

3.1 Microstructural heterogeneity of dispersoids

The representative SEM micrographs of the air-cooled 6082-H and 6082-U alloys are shown in Figs. 1(a, b) and 1(d, e), respectively, revealing the heterogeneous distribution of dispersoids due to the absence of homogenization before extrusion. Elongated bands of dispersoid-free zones (DFZs) with an average width of (1.72±0.25) μm parallel to the extrusion direction can be observed in the 6082-U alloy (Figs. 1(a, b)). Similar phenomenon is usually observed in Mn-containing Al alloys [22,33] as a result of Mn segregation during solidification [22,26]. In contrast, homogenization prior to extrusion effectively eliminates the heterogeneity of dispersoids in the 6082-H alloy, resulting in a roughly homogeneous microstructure, as shown in Figs. 1(d, e). The microstructural parameters of the dispersoids are presented in Table 2.

Furthermore, TEM characterizations were conducted at higher magnifications on these alloys (see Figs. 1(c, f)). Interestingly, it is found that lath-like particles decorate the majority of α-Al(Fe,Mn)Si dispersoids in two studied air-cooled alloys. Careful EDS examinations reveal clear Si, Mn and Fe depletion within these DFZs (Figs. 2(a−f)), while corresponding second-phase particles within adjacent dispersoid-containing zones (DZs) show solute enrichment, indicating that

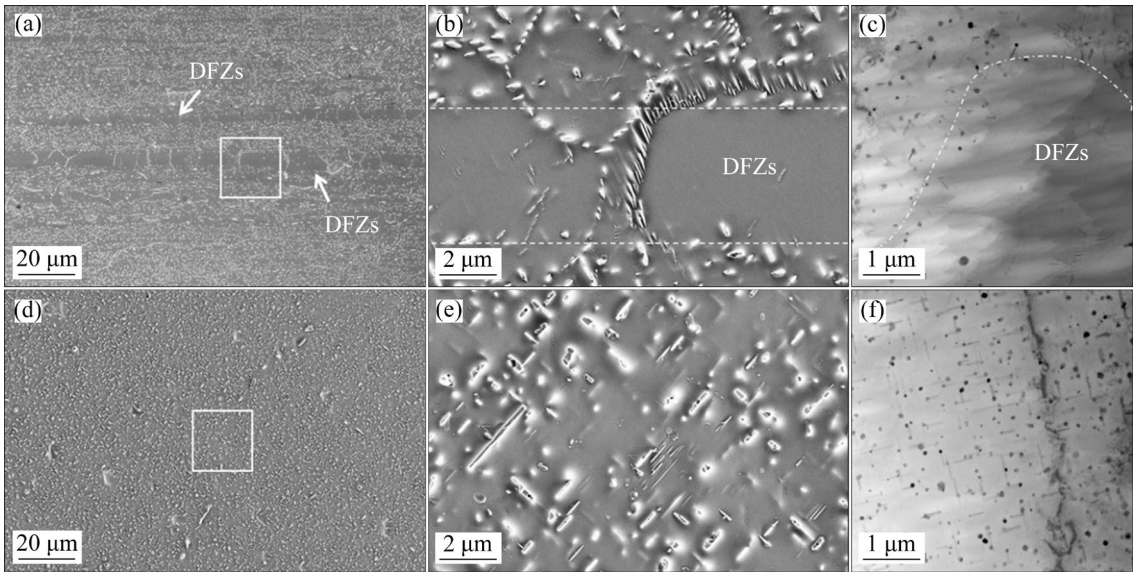

Fig. 1 Microstructure of air-cooled 6082-U (a−c) and 6082-H (d−f) alloys showing heterogeneity of α-Al(Fe,Mn)Si dispersoids: (a, b, d, e) SEM images; (c, f) TEM images

Table 2 Statistical data of α-Al(Fe,Mn)Si dispersoids and β'' precipitates in studied alloys

Alloy	Location	α-Al(Fe,Mn)Si dispersoids		β'' precipitates			
		$\bar{d}$ /nm	$N_v/10^{19}m^{-3}$	$\bar{l}$ /nm	$\bar{r}$ /nm	$N_v/10^{22}m^{-3}$	f_v/%
6082-U (Air-cooled)	DFZs	−	−	17.0±3.3	3.4±0.2	4.5±0.3	0.90±0.08*
	DZs	81.6±2.6	6.1±0.4	42.1±7.3	4.3±0.4	0.4±0.1	0.54±0.03*
6082-H (Air-cooled)	−	80.3±0.2	8.3±1.4	20.1±4.5	3.1±0.3	3.6±0.2	0.62±0.11
6082-U (Water-quenched)	DFZs	−	−	18.9±0.3	3.3±0.2	7.6±0.7	1.04±0.03*
	DZs	86.3±3.9	6.3±0.8	19.3±0.4	3.2±0.1	7.9±0.4	0.99±0.06*
6082-H (Water-quenched)	−	94.8±7.2	4.5±1.3	23.2±1.2	2.8±0.3	7.1±0.3	0.98±0.11

* The volume fractions were calculated by assuming that precipitates are uniformly distributed in the material; Microstructural parameters: $\bar{d}$ −Average diameter, $\bar{l}$ −Average length, $\bar{r}$ −Average radius, N_v−Number density, f_v−Volume fraction

the majority of the dispersoids are α-Al(Fe,Mn)Si phases [4].

Additionally, a high population of coarse precipitates at both grain boundaries and interiors are enriched in Mg and Si, which are proposed to be β' and/or equilibrium β phase formed due to slow cooling rate during air-cooling [4,24]. Careful HAADF-STEM analyses along with EDS and HRTEM results confirm that these lath-like particles decorated at α-Al(Fe,Mn)Si dispersoids are identified as β'-Mg_9Si_5 (abbreviated as β' hereafter) (see Fig. 3), which is well-known in air-cooled Al−Mg−Si alloys [4,34]. Additional TEM and EDS examinations also reveal that approximately 90.4% of α-Al(Fe,Mn)Si dispersoids are decorated with β' particles in the 6082-U alloy, while this percentage increases to around 94.4% in its 6082-H counterpart (see Fig. S1 in Supplementary Information). In summary, the heterogeneity of α-Al(Fe,Mn)Si dispersoids can be triggered via the homogenization procedures in the present 6082 alloys.

There is no doubt that the coarse β' particle is not the key contributor of the aging-hardening response due to its coarse size and resultantly large interspace λ [4,35]. In other words, α-Al(Fe,Mn)Si dispersoids have a negative impact on introducing β' precipitation. Therefore, an idea arises: eliminating dispersoids could potentially suppress such dispersoid-induced β' precipitation. This approach may be a sensible strategy to enhance the precipitation strengthening effect in the air-cooled

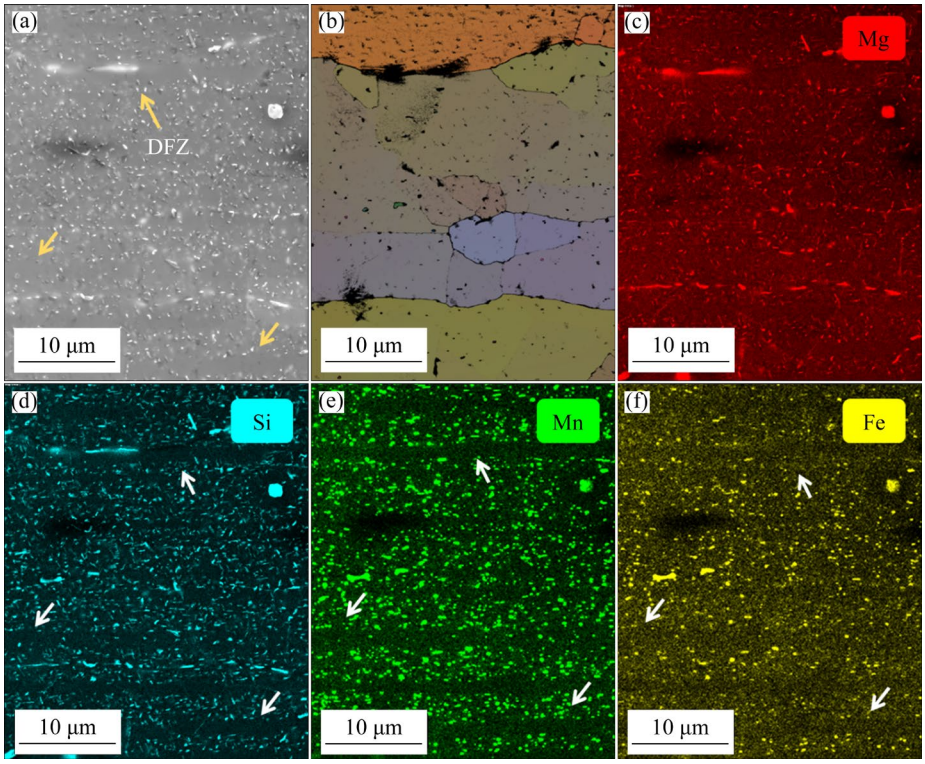

Fig. 2 Dispersoid heterogeneity in 6082-U alloy under higher magnifications: (a) SEM micrograph; (b) Grain orientation distribution in Euler's color; (c−f) Corresponding EDS maps

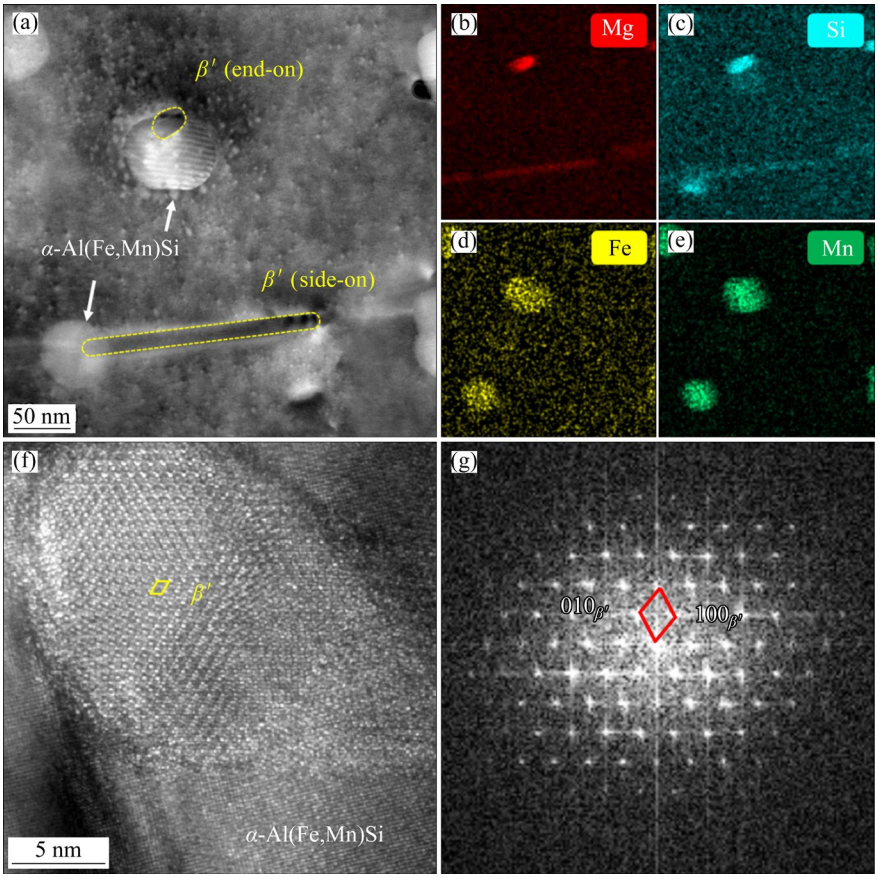

Fig. 3 Heterogeneous nucleation of β' precipitates on α-Al(Fe,Mn)Si dispersoids in 6082-U alloy: (a) HAADF-STEM image; (b−e) Corresponding EDS results; (f) HRTEM image; (g) Corresponding FFT image

alloys. In fact, it should be noted that the precipitation of β'-decorated α-Al(Fe,Mn)Si dispersoid is not observed in the DFZs of the 6082-U alloy after air-cooling, as shown in Fig. 1(c), since there are not dispersoids. Therefore, it is important to carefully characterize the formation of nanoprecipitates in DFZs.

3.2 Microstructural heterogeneity of precipitates cooperating with dispersoids

High-magnified TEM micrographs along with corresponding size distribution of nanoprecipitates in both studied alloys (6082-U and 6082-H) are presented in Fig. 4. Clearly, these TEM micrographs exhibit three variations of nanoprecipitates, including two orthogonal needle-like ones and dot-like end-on variations viewed along $\langle 100\rangle_{Al}$ axis. Further HRTEM and FFT characterizations confirm these particles as β''-Mg_5Si_6 [36,37] or $Mg_5Al_2Si_4$ [21] (abbreviated as β'' hereafter), exhibiting a classic monoclinic structure and representative FFT patterns depicted in Fig. 5, consistent with previous studies [15,20,38,39].

Specifically, if looking back at the microstructural heterogeneity, a surprising fact is found that β'' phases are heterogeneously dispersed in the 6082-U alloy, depending on their distance from α-Al(Fe,Mn)Si dispersoids (see Figs. 4(a, b)). It is noted that such synergetic heterogeneity is almost eliminated in the homogenized 6082-H alloy (see Figs. 4(d, e)). In detail, the 6082-U alloy is equipped with the bimodally distributed β'', which

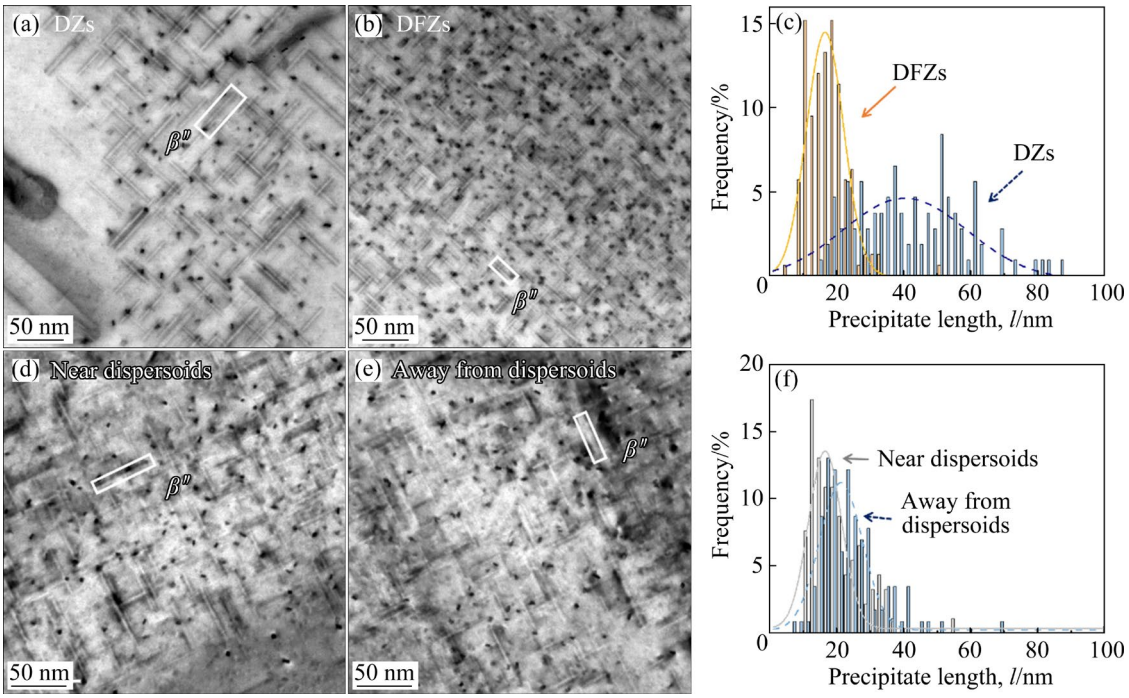

Fig. 4 Heterogeneity of β'' precipitates in 6082-U (a−c) and 6082-H (d−f) alloys: (a, b, d, e) TEM micrographs; (c, f) Size distributions

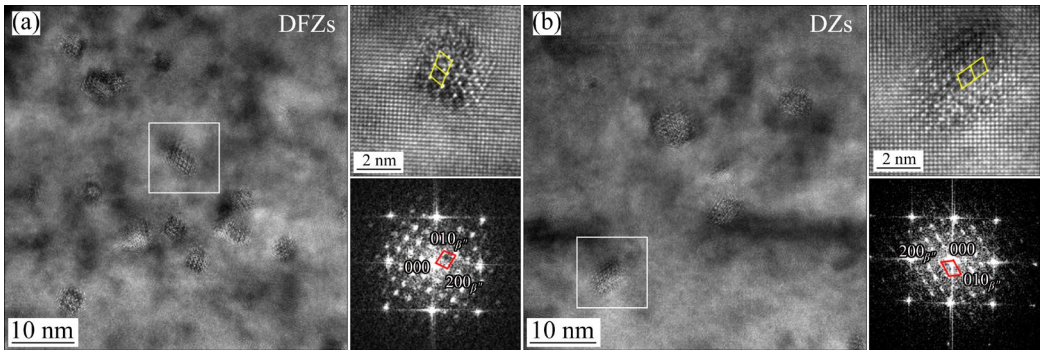

Fig. 5 HRETM and corresponding FFT results identifying β'' precipitates in 6082-U alloy: (a) DFZs; (b) DZs

is in a good agreement with the size distribution in Fig. 4(c). Statistical measurements further clarify that β'' precipitates in the DFZs exhibit ~60% decrease in average length $\bar{l}$ (~17 nm vs ~41 nm) and at least one order of magnitude higher number density N_v (4.5×10^{22} m^{-3} vs 0.4×10^{22} m^{-3}) compared to those found in adjacent DZs. For the purpose of comparison, it is observed in Figs. 4(d−f) that the bimodal distribution of β'' in the 6082-H alloy is nearly eliminated while maintaining unchanged precipitate morphology. An interesting fact is also noticed that the average length l of needle-like β'' in the homogenized 6082-H alloy becomes coarser (~20 nm) compared to that in the DFZs of the 6082-U counterpart, accompanied with a significant decrease in number density N_v to ~3.6×10^{22} m^{-3} (see Table 2). This suggests the simultaneously suppressed heterogeneity of α-Al(Fe,Mn)Si dispersoids and β'' precipitates in the homogenized 6082-H alloy. Conversely, considering the heterogeneous microstructure present in the unhomogenized 6082-U alloy, it is found that there exists a surprising synergy of heterogeneity regarding to α-Al(Fe,Mn)Si and β'' particles. In brief, the spatial distributions of α-Al(Fe,Mn)Si dispersoids and β'' precipitates are either homogenous or heterogeneous in the air-cooled 6082 alloys.

3.3 Mechanical properties

Figure 6(a) shows the representative room-temperature engineering stress−strain curves of the studied 6082-U and 6082-H alloys through air-cooling. Clearly, the yield strength ($\sigma_{0.2}$) and ultimate strength (σ_b) are obviously upgraded from ~170 and ~230 MPa in the 6082-H alloy to ~190 and ~255 MPa in the unhomogenized 6082-U alloy, respectively. The refined β'' precipitates in the DFZs are attributed to the strong strengthening effect in the unhomogenized 6082-U alloy. It is worth noting that such improved strength seems to be not valid in the water-quenched alloys (see Fig. S2 in Supplementary Information). However, the utilization of microstructural heterogeneity (schematically presented in Figs. 6(b, c)) is still important for these air-cooled alloys from the perspective of the highly restricted precipitation strengthening effect due to the slow cooling rate.

Meanwhile, the ductility is also optimized from ~11% in the 6082-H alloy to ~15% in the 6082-U counterpart. The underlying mechanism can be explained as follows. The microstructural heterogeneity of α-Al(Fe,Mn)Si dispersoids and β'' precipitates actually assembles a composite structure stratified by multiple “hard” and “soft” layers in micro-scale. These layers correspond to the assembly of DFZs with refined precipitates and DZs with dispersoids and coarser precipitates. Similar laminated and heterostructured materials with microstructural heterogeneity have been proven to possess desirable strength−ductility synergy [40]. For example, a recent work proposed by ZHAO et al [41] shows a similar heterogeneous sandwiched microstructure within an ultra-thin Al−Mn strip. A mutual constraint between the hard and soft regions is found to enable the material to be plastically deformed to an elongation increased by ~200% prior to fracture. Based on these analyses, DFZs are likely to be the “hard” part of alloy due to the refined β'' precipitation. Moreover, another possible explanation for the optimized ductility in the unhomogenized 6082-U alloy is

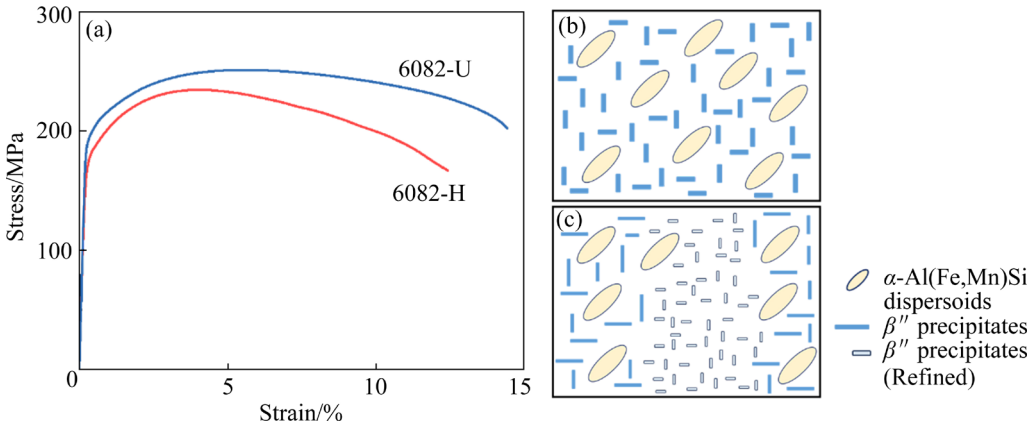

Fig. 6 Mechanical properties of studied alloys: (a) Room-temperature tensile curves; (b, c) Schematics presenting synergetic heterogeneity in 6082-H (b) and 6082-U (c) alloys

related to the β'' precipitates with smaller size in the DFZs, which is supposed to reduce the deformation discrepancy between the precipitate and matrix and thus to decrease the strain/stress concentration [6,42,43]. However, it seems to be less important because the coarser precipitates are also observed in DZs and resultantly jeopardize the ductility. Unfortunately, the improved mechanical property by skipping homogenization seems to be not effective in the water-quenched counterpart (see Fig. S2 in Supplementary Information). Therefore, the microstructural heterogeneity is most likely to be responsible for optimal strength and ductility combination processed by the unhomogenized 6082-U alloy.

4 Discussion

4.1 Heterogeneous precipitation of α-Al(Fe,Mn)Si dispersoids

The heterogeneity of the α-Al(Fe,Mn)Si dispersoids is associated with the Mn segregation during solidification and inherited in the unhomogenized 6082-U alloy. For instance, the Mn enrichment is detected in dendritic core [22,26] of cast alloys, and the surface region of twin-roll casting (TRC) strip [2,41]. These are well-known macroscopic or microscopic defects, i.e. center segregation [44]. Efforts have been made to eliminate or mitigate these defects by optimizing fabrication processes or controlling thermo-mechanical procedures. However, in this work, the microstructural heterogeneity of α-Al(Fe,Mn)Si dispersoids is intentionally allowed in the present 6082-U alloy by skipping the homogenization step before extrusion, and the DFZs are consequently produced. In addition, the areas with a lower population density of dispersoids, namely the DFZs, are deformed during the extrusion, which consequently leads to the formation of the DFZs in form of bands following the extrusion direction, as shown in Figs. 1(a, b).

For a quantitative purpose, we can simply use the solute diffusion distance to evaluate the threshold condition of eliminating the DFZs in present alloys. The root mean diffusion distance law [45] is utilized, i.e., $x=\sqrt{4D_i t}$, where x is the root-mean-square (RMS) diffusion distances, t is the duration of homogenization and D_i is the diffusion coefficient of relevant solutes (Mg, Si, Fe and Mn) in Al matrix. It is noted that the values of D_i are calculated by following the classic Arrhenius-type relationship ($D_i=D_0\exp[-Q_i/(RT)]$) [46], where D_0 and Q_i are denoted as the pre-exponential factor and the activation energy for solute i (i=Mg, Si, Fe and Mn) [46], R is the molar gas constant and T is the thermodynamic temperature. For our 6082-U and 6082-H alloys, T is chosen as 480 °C (~753 K) as the homogenization temperature, and the corresponding results are plotted in Figs. 7(a, b). Clearly, the homogenization of Mn is much more difficult compared to that of Mg, Si and even Fe due to its sluggish diffusion, as shown in Fig. 7(a). However, if performing the homogenization procedure at 480 °C for 4 h, the value of diffusion distance x for Mn is further increased to ~1.3 μm. Such value is very close to the average width of DFZs (~1.7 μm) in the unhomogenized 6082-U alloy. This implies that the solute diffusion of Mn can be thermally activated by the homogenization procedure to eliminate the heterogeneity of Mn-rich dispersoids.

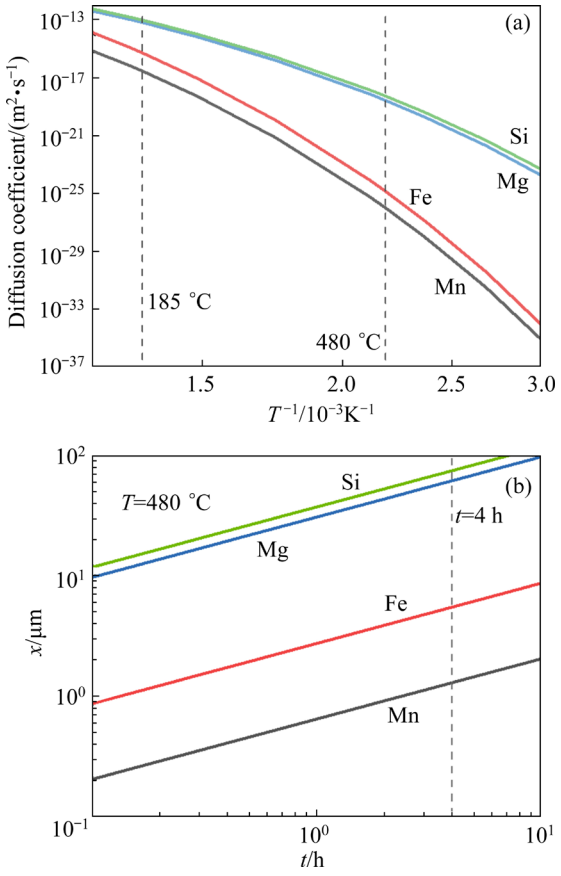

Fig. 7 Diffusivities of Mg, Si, Mn and Fe in Al matrix: (a) Diffusion coefficients as function of inverse temperature; (b) Root-mean-square (RMS) diffusion distances (x) at 480 °C as function of time (t)

In fact, such prediction is confirmed by the experimental results in Fig. 1.

To sum up, the above calculations on solute diffusion rationalize the presence of DFZs in the unhomogenized 6082-U alloys and its elimination in the 6082-H alloy by the homogenization protocol, as observed in Figs. 1(c, d).

4.2 Heterogeneous precipitation of β'' precipitates

Generally, the needle-like β'' precipitates are considered as the most efficient strengthening phase in Al−Mg−Si alloys [21,30,36,38]. In the present 6082-U alloy, the reason why the heterogeneity of β'' precipitation and α-Al(Fe,Mn)Si dispersoids remains synergetic still requires further discussion. Apparently, the segregation of Mg and Si during solidification can be easily eliminated at relatively high temperature and is thus excluded here (based on the calculations on the solute diffusion in Section 4.1). However, solute competition between β'' precipitates and α-Al(Fe,Mn)Si dispersoids (as well as the heterogeneously nucleated β' phases) needs to be taken into account.

Mg and Si compositions in the DFZs and DZs of the 6082-U alloy were analysed by using EDS detectors in TEM (see Fig. S3 in Supplemental Information). A minimum of 5 spots were generated for comparison in each type of domain. Here, there are distinctive differences in Si contents in the DFZs (~0.7 at.%) and in the DZs (~0.5 at.%) in the 6082-U alloy, while Mg contents are quite similar (~0.4 at.%). In other words, the DZs exhibit a decreased Si content in comparison to the adjacent DFZs with a reduced amount of dispersoids. This can be easily related to the Si competition between β'' precipitates and α-Al(Fe,Mn)Si dispersoids, which is irrelevant to Mg. On the one hand, the abundant solutes are provided for precipitation in the DFZs, thus resulting in a higher volume fraction of β'' than that in the DZs. On the other hand, the excess Si (high Si/Mg ratio) has been proved to encourage rapid (Mg,Si)-rich precipitation by accelerating clustering and phase transition to β'' [12]. Thus, the Si fluctuation between DFZs and DZs rationalizes the promoted β'' precipitates in DFZs of the unhomogenized 6082-U alloy and the synergetic heterogeneity of these two strengthening phases by solute competition.

Furthermore, another factor is also provided as a potential mechanism of the heterogeneity of β'': the solute competition between β'' and β'. Due to the absent α-Al(Fe,Mn)Si in DFZs, the Mg and Si solutes are therefore less consumed by β' nucleated on dispersoids during air quenching. Hence, an increasing number of refined β'' precipitates is consequently acquired, which possesses the enhanced age-hardening response relative to the adjacent DZs in the alloy. In fact, the β' precipitation nucleated on α-Al(Fe,Mn)Si dispersoids is indeed found in present air-cooled 6082-U and 6082-H alloys, as shown in Figs. 3 and 4.

It is necessary to discuss the effect of β' precipitation on the formation of β''. In previous studies, however, the β' precipitation promoted by the α-Al(Mn,Fe)Si dispersoids has well-known detrimental influence on suppressing the β'' precipitation in air-cooled Al−Mg−Si alloys [4]. This results in the reduced strength of the material. In contrast, this work shows that such effect seems to be comparable (and even more important) when compared to the Si depletion directly caused by α-Al(Fe,Mn)Si dispersoids based on two possible mechanisms:

(1) In the present air-cooled alloys, coarse β'' precipitates are seldomly observed at the periphery of β'-decorated α-Al(Fe,Mn)Si dispersoids (see highlights in Fig. 4(e)). This suggests that the localized Mg and Si depletion is induced by the β' precipitation. However, such heterogeneity is limited in very narrow regions (within tens of nanometres in radius) and quickly eliminated to resume the normal size of β'' widely dispersed in matrix. This kind of microstructural feature hardly jeopardizes the strengthening and, however, may be helpful to improve the ductility by relieving the stress/strain concentration between precipitates and dispersoids due to the relatively large inter-particle spacing [6,42,43].

(2) Further experiments on the water-quenched alloys show that the heterogeneity of β'' is completely vanished whether the alloy is homogenized or not (see Figs. 8(a−h)). As a result, the heterogeneous β'' precipitation with fair size (Fig. 8 and Table 2) in the water-quenched 6082-U and 6082-H alloys finally leads to the similar strength (see Fig. S2 in Supplementary Information). Such results clarify that the β' phase is also the key competitor with β'' to consume alloying elements to tune its heterogeneity. To be brief, heterogeneously β' precipitation also plays crucial roles in tuning the

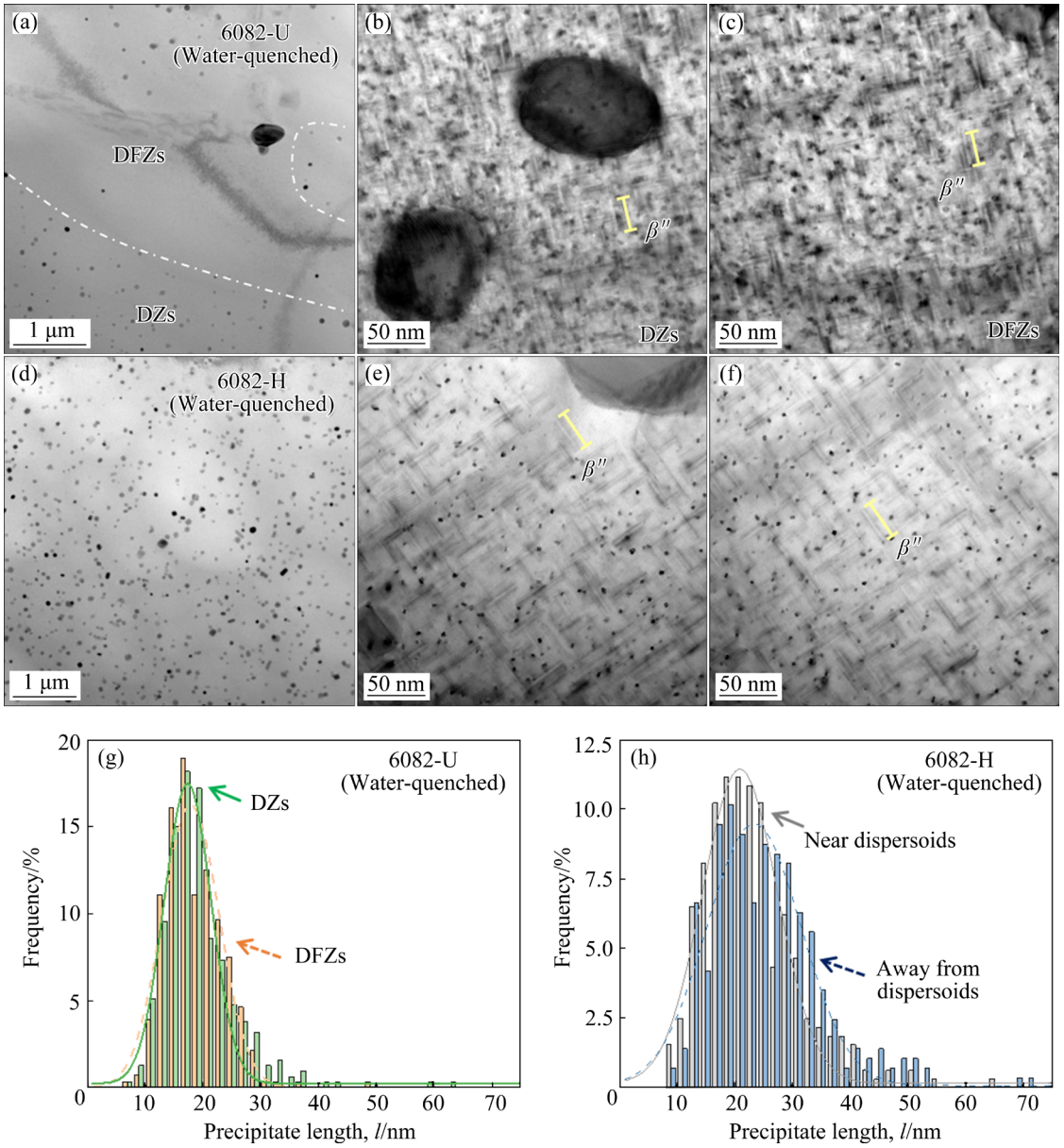

Fig. 8 Invalid heterogeneity of α-Al(Fe,Mn)Si dispersoids and β'' precipitates in water-quenched 6082-U (a−c, g) and 6082-H (d−f, h) alloys: (a−f) TEM micrographs; (g, h) Size distributions of β'' precipitates

synergy of microstructural heterogeneity of α-Al(Fe,Mn)Si and β'', which is promoted by the preferred nucleation sites by the former and subsequently triggers the limited solute supplying for the later. In contrast, the DFZs benefit from the absence of dispersoids and are thus equipped with refined β'' precipitates with large volume fraction.

4.3 Strengthening model

Theoretically, strengthening effect contributed by dispersoids and nanoprecipitates mainly comes from the interaction between them with the dislocations, quantitively depended on the micro-parameters including size (i.e. length l and radius r for β'' precipitates), number density N_v and volume fraction f_v. In this section, the strengthening increment contributed by α-Al(Fe,Mn)Si dispersoids ($\Delta\sigma_{dis}$) and β'' nanoprecipitates ($\Delta\sigma_{\beta''}$) is quantitively evaluated.

For α-Al(Fe,Mn)Si dispersoids, the strengthening increment $\Delta\sigma_{dis}$ can be calculated as [35]

$$\Delta\sigma_{dis}=\frac{MF}{b\lambda} \tag{1}$$

where M and b are the Taylor's factor (~3.06 [47]) and magnitude of Burgers vector (~0.286 nm [47]), respectively; F is the force for the dislocations to

bypass the dispersoid (Orowan looping), which follows the expression of $F=Gb^2$ (where G is the shear modulus of aluminum) [35]; λ is the interspace of dispersoids and expressed as $\lambda=(2/3\pi/f_v)^{0.5}(d/2)$ (d is the average particle size) [48]. In the present alloys, the similar strengthening increment contributed by dispersoids can be therefore estimated as ~32.1 and ~38.9 MPa for the air-cooled 6082-U and 6082-H alloys, respectively, by using the microstructural parameters presented in Table 2. By considering the statistical error of measurements, it is then implied that heterogeneity of dispersoids, in fact, is not responsible for the improved strength in the air-cooled 6082-U alloy in comparison to its homogenized 6082-H counterpart, as also compared in a series of theoretical estimations in Fig. 9(a). Therefore, the heterogeneous nanoprecipitations are regarded as the key factor of the improved mechanical property.

However, for the $\{100\}_{Al}$ needle-shaped β'' precipitates, the strengthening mechanisms of shearing and Orowan looping should be considered [49]. The critical radius r_c of β'' precipitates for shearing mechanism switching to Orowan looping mechanism is claimed to be about 3.0−4.0 nm at room temperature [36,38,49]. Here, we adopt a medium value of 3.5 nm. It is noted that the similar transition radius is also proposed by POOLE et al [35]. Accordingly, the β'' phases in the 6082-H and DFZs in 6082-U alloys with r of ~3.0 nm should be regarded to be shearable, while the relatively coarser precipitates in the DZs of the 6082-U alloy (~4.1 nm) are unshearable. The detailed equations are presented as follows.

(1) The strengthening contribution of shearable β'' ($\Delta\sigma_{\beta''}^{sh}$) can be estimated by following equations [36,49]:

$$\Delta\sigma_{\beta''}^{sh}=\Delta\sigma_{ord}+\Delta\sigma_{mod}+\Delta\sigma_{coh} \quad (2)$$

$$\Delta\sigma_{ord}=\frac{M\gamma}{2b}\left(\frac{3\pi^2\gamma f_v r}{16Gb^2}\right) \quad (3)$$

$$\Delta\sigma_{mod}=0.0055M(\Delta G)^{\frac{3}{2}}\left(\frac{2f_v}{Gb^2}\right)^{\frac{1}{2}}b\left(\frac{r}{b}\right)^{\frac{3m}{2}-1} \quad (4)$$

$$\Delta\sigma_{coh}=\alpha_\varepsilon M(G\varepsilon)^{\frac{3}{2}}\left(\frac{2f_v r}{Gb}\right)^{1/2} \quad (5)$$

where G=26.9 GPa [50]; α_ε (=2.6) and m (=0.85) are constants, referring to Ref. [48]; r is the mean radius of β'' particles, referring to statistical data in Table 2; γ is the interfacial energy of β''/Al interface (0.08 J/m^2 [51]); lattice strain $\varepsilon\approx 2/3\delta$ [48], and δ (≈2.1%) is the fractional misfit between the lattice parameters of β'' precipitates and Al matrix [36]; ΔG (=42.5 GPa) is the shear modulus mismatch between Al matrix and β'' precipitates.

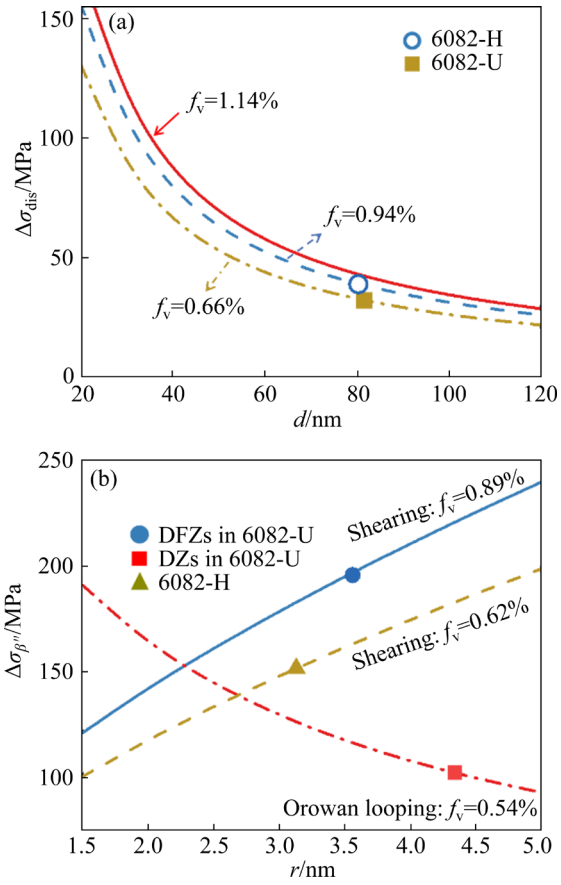

Fig. 9 Theoretical prediction of strengthening increment of α-Al(Fe,Mn)Si dispersoids ($\Delta\sigma_{dis}$) (a) and β'' precipitates ($\Delta\sigma_{\beta''}$) (b) as function of average particle size

(2) The main strengthening increment of unshearable β'' ($\Delta\sigma_{\beta''}^{oro}$) follows the expression [49]:

$$\Delta\sigma_{\beta''}^{oro}=\frac{0.15MGb}{2r}\cdot[f_v^{1/2}+1.84f_v+1.84f_v^{3/2}]\ln\left(\frac{2.632r}{r_0}\right) \quad (6)$$

where r_0 (≈0.572 nm) is the inner cut-off radius for the calculation of the dislocation line tension [52].

By using Eqs. (1)−(6)), the theoretical models predict that the strength increment by refined β'' precipitates in DFZs of the 6082-U alloy is ~190 MPa, which is much greater than that in DZs and heterogeneous precipitation in the 6082-H alloy (~137 MPa and ~150 MPa, respectively) (see

Fig. 9(b)). The calculation results strongly support the conclusion that the assembly of DFZs and DZs actually forms the "hard" and "soft" domains in the heterostructured 6082-U alloy, as accomplished by skipping homogenization. According to ZHU et al [40], the hard domains (i.e. DFZs in the 6082-U alloy) are prone to remain elastic, and back stress plays a dominant role in enhancing the global yield strength in the material, which possesses superior combinations of strength and ductility. This is in good agreement with the experimental results of improved strength in the unhomogenized 6082-U alloy shown in Fig. 6(a).

5 Conclusions

(1) The unhomogenized 6082-U alloy exhibits a synergetic heterogeneity of α-Al(Fe,Mn)Si dispersoids and β'' precipitates. On the one hand, the heterogeneous spatial distribution of α-Al(Fe,Mn)Si dispersoids is primarily attributed to Mn segregation inherited from the as-cast ingots, resulting in a large number of dispersoid-free zones (DFZs). On the other hand, the heterogeneous β'' precipitates are simultaneously acquired, leading to refined β'' precipitates in the DFZs relative to adjacent DZs.

(2) The synergetic heterogeneity of the dispersoids and nanoprecipitates is responsible for the improved strength−ductility synergy in the unhomogenized 6082-U alloy compared to the homogenized 6082-H counterpart. The heterogeneity of α-Al(Fe,Mn)Si dispersoids plays a key role in triggering the heterogeneous distribution of β'' precipitation by creating solute competitions among multiple second-phase particles.

(3) A strengthening model is employed to quantitively evaluate the strengthening effect contributed by dispersoids and nanoprecipitates by considering their microstructural heterogeneity.

CRediT authorship contribution statement

Yi-han GAO: Conceptualization, Investigation, Methodology, Formal analysis, Writing – Original draft, review and editing, Funding acquisition; **Xin-xin ZHANG:** Conceptualization, Formal analysis, Methodology, Data curation, Funding acquisition, Writing – Review & editing; **Jing-zhe ZHOU:** Conceptualization, Methodology, Data curation, Investigation, Formal analysis; **Peng XU:** Formal analysis; **Zhi-jie XIN:** Formal analysis, Project administration; **Jun-hua GAO:** Formal analysis; **Yan-hao SHI:** Formal analysis; **You LÜ:** Formal analysis; **Yu-fang ZHAO:** Conceptualization, Investigation, Data curation, Funding acquisition, Writing – Review & editing; **Jing-yang LI:** Conceptualization, Resources, Supervision, Writing – Review & editing.

Declaration of competing interest

The authors declare that they have no known competing financial interests or personal relationships that could have appeared to influence the work reported in this paper.

Acknowledgments

This work was supported by the National Natural Science Foundation of China (Nos. 52301025, 52371065, 52301179) and the Fundamental Research Program of Shanxi Province, China (Nos. 202203021222039, 202203021212124). The authors thank the technical supports from Analytical and Testing Centre in Huazhong University of Science and Technology (HUST) and Experiment Centre for Advanced Manufacturing and Technology in School of Mechanical Science & Engineering of HUST, China. We also thank Y. C. WU, Y. QIN and Z. Z. CAI at the electron microscope center of KAIPLE Co. Ltd. (KAIPLE EMC, Changsha, China), Mr. Z. B. ZHANG at North University of China and the Instrumental Analysis & Research Centre of Shanghai Yanku (www.shuyanku.com) (China) for their great assistance of TEM and SEM analyses.

Supplementary Information

Supplementary Information in this paper can be found at: http://tnmsc.csu.edu.cn/download/01-p1017-2023-0906-Supplementary_Information.pdf.

References

[1] POGATSCHER S, ANTREKOWITSCH H, LEITNER H, EBNER T, UGGOWITZER P J. Mechanisms controlling the artificial aging of Al−Mg−Si Alloys [J]. Acta Materialia, 2011, 59: 3352−3363.

[2] KUANG Jie, ZHAO Xiao-long, ZHANG Yu-qing, ZHANG Jinyu, LIU Gang, SUN Jun, Xu Guang-ming, WANG Zhao-dong. Impact of thermal exposure on the micro-structure and mechanical properties of a twin-roll cast Al−Mn−Fe−Si strip [J]. Journal of Materials Science & Technology, 2022, 107: 183−196.

[3] ZHANG Shao-you, WANG Xuan, MO Yuan-ting, WANG Cheng, CHENG Tuo, IVASISHIN O, MA Pin-kui, WANG Hui-yuan. Towards relieving center segregation in twin-roll

cast Al−Mg−Si−Cu strips by controlling the thermal-mechanical process [J]. Journal of Materials Science & Technology, 2023, 148: 31−40.

[4] RAKHMONOV J, LIU K, ROMETSCH P, PARSON N, CHEN X G. Effects of Al(MnFe)Si dispersoids with different sizes and number densities on microstructure and ambient/elevated-temperature mechanical properties of extruded Al–Mg−Si AA6082 alloys with varying Mn content [J]. Journal of Alloys and Compounds, 2021, 861: 157937.

[5] ZHAO Hai-xiao, SUN Lu, ZHAO Guo-qun, YU Jun-quan, LIU Fei, SUN Xi-man, LV Zheng-feng, CAO Shan-peng. Abnormal grain growth behavior and mechanism of 6005A aluminum alloy extrusion profile [J]. Journal of Materials Science & Technology, 2023, 157: 42−59.

[6] LIU Gang, ZHANG Guo-jun, WANG Rui-hong, HU Wei, SUN Jun, CHEN Kang-hua. Heat treatment-modulated coupling effect of multi-scale second-phase particles on the ductile fracture of aged aluminum alloys [J]. Acta Materialia, 2007, 55: 273−284.

[7] SCHMID F, WEIßENSTEINER I, TUNES M A, KREMMER T, EBNER T, MORAK R, UGGOWITZER P J POGATSCHER S. Synergistic alloy design concept for new high-strength Al−Mg−Si thick plate alloys [J]. Materialia, 2021, 15: 100997.

[8] SUN Teng-teng, GENG Ji-wei, BIAN Ze-yu, WU Yi, WANG Ming-liang, CHEN Dong, MA Nai-heng, WANG Hao-wei. Enhanced thermal stability and mechanical properties of high-temperature resistant Al−Cu alloy with Zr and Mn micro-alloying [J]. Transactions of Nonferrous Metals Society of China, 2022, 32: 64−78.

[9] DONG Fang, ZHANG Tao, WU Yun-xin, LIU Lei, HAO Tie-wen. Multi-scale simulation of flow behavior and microstructure evolution for AA2219 alloy during multi-pass ring rolling process [J]. Transactions of Nonferrous Metals Society of China, 2023, 33: 2926−2942.

[10] ZHANG Meng-han, LIU Sheng-dan, JIANG Jing-yu, WEI Wei-chang. Effect of Cu content on intergranular corrosion and exfoliation corrosion susceptibility of Al−Zn−Mg−(Cu) alloys [J]. Transactions of Nonferrous Metals Society of China, 2023, 33: 1963−1976.

[11] YUAN Liang-liang, GUO Ming-xing, YAN Yong, FENG Wei-jun, LIU Zan-yang, ZHUANG Lin-zhong. Theoretical design and distribution control of precipitates and solute elements in Al−Zn−Mg−Cu alloys with heterostructure [J]. Transactions of Nonferrous Metals Society of China, 2021, 31: 3328−3341.

[12] JIANG Sheng-yu, WANG Rui-hong, Grain size-dependent Mg/Si ratio effect on the microstructure and mechanical/electrical properties of Al−Mg−Si−Sc alloys [J]. Journal of Materials Science & Technology, 2019, 35: 1354−1363.

[13] WEI Bo, PAN Shuai, LIAO Gui-zhen, ALI A, WANG Shuang-bao. Sc-containing hierarchical phase structures to improve the mechanical and corrosion resistant properties of Al−Mg−Si alloy [J]. Materials & Design, 2022, 218: 110699.

[14] BOCHVAR N R, RYBALCHENKO O V, TABACHKOVA N Y, RYBALCHENKO G V, LEONOVA N P, ROKHLIN L L. Kinetics of phase precipitation in Al−Mg−Si alloys subjected to equal-channel angular pressing during subsequent heating [J]. Journal of Alloys and Compounds, 2021, 881: 160583.

[15] JIN Hong-mei, TIE Di, GUAN Ren-guo. Precipitation behavior during re-aging of Al−Mg−Si−Cu alloy [J]. Materials & Design, 2022, 220: 110883.

[16] WU Xian, GUAN Zhi-ping, YANG Zhi-zheng, WANG Xuan, QIU Feng, WANG Hui-yuan. Effect of Cu content on central-segregation composition and mechanical properties of Al−Mg−Si alloys produced by twin-roll casting [J]. Materials Science and Engineering A, 2023, 869: 144782.

[17] ÅNES HÅKON W, van HELVOORT ANTONIUS T J, MARTHINSEN K. Orientation dependent pinning of (sub) grains by dispersoids during recovery and recrystallization in an Al−Mn alloy [J]. Acta Materialia, 2023, 248: 118761.

[18] NAGAUMI H, QIN J, YU Cheng-bin, WANG Xiao-guo, WANG Lin-sheng. Quantitative analysis of influence of α-Al(MnFeCr)Si dispersoids on hot deformation and microstructural evolution of Al−Mg−Si alloys [J]. Transactions of Nonferrous Metals Society of China, 2022, 32: 1805−1821.

[19] WANG Yu-cheng, YANG Tong, LU Qiang, LI Kai, WANG Zhi-xiu, DU Yong. Grain size refinement and enhanced precipitation strengthening in a hot extruded 6xxx Al alloy without homogenization [J]. Materials Characterization, 2023, 198: 112718.

[20] van HUIS M A, CHEN J H, SLUITER M H F, ZANDBERGEN H W. Phase stability and structural features of matrix-embedded hardening precipitates in Al−Mg−Si alloys in the early stages of evolution [J]. Acta Materialia, 2007, 55: 2183−2199.

[21] LU Qiang, LI Kai, CHEN Hao-nan, YANG Ming-jun, LAN Xin-yue, YANG Tong, LIU Shu-hong, SONG Min, CAO Ling-fei, DU Yong. Simultaneously enhanced strength and ductility of 6xxx Al alloys via manipulating meso-scale and nano-scale structures guided with phase equilibrium [J]. Journal of Materials Science & Technology, 2020, 41: 139−148.

[22] LIU K, MA H Z Y, CHEN X G. Enhanced elevated-temperature properties via Mo addition in Al−Mn−Mg 3004 alloy [J]. Journal of Alloys and Compounds, 2017, 694: 354−365.

[23] WANG Yu-chi, FREIBERG D, HUO Yang, ZHU Wen-hui, WILLIAMS R, LI Mei, WANG Yun-zhi. Shapes of nano Al6Mn precipitates in Mn-containing Al-alloys [J]. Acta Materialia, 2023, 249: 118819.

[24] MILKEREIT B, STARINK M J. Quench sensitivity of Al−Mg−Si alloys: A model for linear cooling and strengthening [J]. Materials & Design, 2015, 76: 117−129.

[25] CAVAZOS J L, COLÁS R. Quench sensitivity of a heat treatable aluminum alloy [J]. Materials Science and Engineering A, 2003, 363: 171−178.

[26] LI Qi-lei, HUANG Guang-jie, CAO Yu, JIA Zhi-hong, HE Jie, LIANG Zi-man, LIU Qing. Enhancement in dispersoid precipitation and dispersion strengthening by prior deformation in an Al−Mg−Mn alloy [J]. Materials Science and Engineering A, 2023, 869: 144808.

[27] LIU Fang-zhen, ZHU Xiao-hua, QIN Jian, ZHOU Wei, LING Jian-quan, DONG Qi-peng, YU Jia-min, NAGAUMI H, ZHANG Bo. Effect of Mn/Cr ratio on precipitation

behaviors of α-Al(FeMnCr)Si dispersoids and mechanical properties of Al−Mg−Si−Cu alloys [J]. Materials Science and Engineering A, 2022, 860: 144269.

[28] MCALISTER A J, MURRAY J L. The (Al−Mn) aluminum−manganese system [J]. Journal of Phase Equilibria, 1987, 8: 438−447.

[29] LI Y J, ARNBERG L. Quantitative study on the precipitation behavior of dispersoids in DC-cast AA3003 alloy during heating and homogenization [J]. Acta Materialia, 2003, 51: 3415−3428.

[30] LI Kai, IDRISSI H, SHA Gang, SONG Min, LU Jiang-bo, SHI Hui, WANG Wan-lin, RINGER S P, DU Yong, SCHRYVERS D. Quantitative measurement for the microstructural parameters of nano-precipitates in Al−Mg−Si−Cu alloys [J]. Materials Characterization, 2016, 118: 352−362.

[31] ZHANG Xin-xin, LV You, LIU Bing, ZHOU Xiao-rong, ZHANG Tong, GAO Yi-han, DONG Ze-hua, WANG Jun-jie, NILSSON J O. The influence of room temperature storage on intergranular corrosion susceptibility of AA6082 Al−Mg−Si alloy [J]. Corrosion Communications, 2021, 3: 71−79.

[32] GAO Yi-han, YANG Chong, ZHANG Jin-yu, CAO Ling-fei, LIU Gang, SUN Jun, MA E. Stabilizing nanoprecipitates in Al−Cu alloys for creep resistance at 300 °C [J]. Materials Research Letters, 2019, 7: 18−25.

[33] LIU Xu, MA Yin-long, WANG Xuan, ZHANG Shao-you, ZHANG Ming-xue, WANG Hui-yuan. Enhanced long-term thermal stability and mechanical properties of twin-roll cast Al−Mg−Si alloys with Mn and Cu additions [J]. Materials Science and Engineering A, 2023, 872: 144945.

[34] HE Yi, XI Hai-hui, MING Wen-quan, SHAO Qin-qin, SHEN Ruo-han, LAI Yu-xiang, WU Cui-lan, CHEN Jiang-hua. Thermal stability and precipitate microstructures of Al−Si−Mg−Er alloy [J]. Transactions of Nonferrous Metals Society of China, 2021, 31: 1−10.

[35] POOLE W J, WANG X., EMBURY J D, LLOYD D J. The effect of manganese on the microstructure and tensile response of an Al−Mg−Si alloy [J]. Materials Science and Engineering A, 2019, 755: 307−317.

[36] YANG Ming-jun, CHEN Hao-nan, OREKHOV A, LU Qiang, LAN Xin-yue, LI Kai, ZHANG Shu-yan, SONG Min, KONG Yi, SCHRYVERS D, DU Yong. Quantified contribution of β'' and β' precipitates to the strengthening of an aged Al–Mg–Si alloy [J]. Materials Science and Engineering A, 2020, 774: 138776.

[37] LEI Gang, GAO Hai-tao, ZHANG Yun, CUI Xiao-hui, YU Hai-liang. Atomic-level insights on enhanced strength and ductility of Al−Mg−Si alloys with β''-Mg_5Si_6 at cryogenic temperatures [J]. Transactions of Nonferrous Metals Society of China, 2023, 33: 2943−2954.

[38] YANG Ming-jun, OREKHOV A, HU Zhi-yi, FENG Man, JIN Shen-bao, SHA Gang, LI Kai, SAMAEE V, SONG Min, DU Yong, VAN TENDELOO, SCHRYVERS D. Shearing and rotation of β'' and β' precipitates in an Al−Mg−Si alloy under tensile deformation: In-situ and ex-situ studies [J]. Acta Materialia, 2021, 220: 117310.

[39] WENG Yao-yao, JIA Zhi-hong, DING Li-peng, LIAO Jin, ZHANG Ping-ping, XU Ya-qi, LIU Qing. Effect of pre-straining on structure and formation mechanism of precipitates in Al−Mg−Si−Cu alloy [J]. Transactions of Nonferrous Metals Society of China, 2022, 32: 436−447.

[40] ZHU Yun-tian, AMEYAMA K, ANDERSON P M, BEYERLEIN I J, GAO Hua-jian, KIM H S, LAVERNIA E, MATHAUDHU S, MUGHRABI H, RITCHIE R O, TSUJI N, ZHANG Xiang-yi, WU Xiao-lei. Heterostructured materials: Superior properties from hetero-zone interaction [J]. Materials Research Letters, 2021, 9: 1−31.

[41] ZHAO Xiao-long, KUANG Jie, SHI Kun-kun, ZHANG Peng, XUE Hang, ZHANG Jin-yu, LIU Gang, SUN Jun, XU Guang-ming, WANG Zhao-dong. Heterogeneous micro-structure-mediated ductile fracture of twin-roll cast Al−Mn strip [J]. Materials Science and Engineering A, 2020, 783: 139222.

[42] LIU Gang, ZHANG Guo-jun, DING Xiang-dong, SUN Jun, CHEN Kang-hua. Modeling the strengthening response to aging process of heat-treatable aluminum alloys containing plate/disc- or rod/needle-shaped precipitates [J]. Materials Science and Engineering A, 2003, 344: 113−124.

[43] LIU Gang, ZHANG Guo-jun, DING Xiang-dong, SUN Jun, CHEN Kang-hua. The influences of multiscale-sized second-phase particles on ductility of aged aluminum alloys [J]. Metallurgical and Materials Transactions A, 2004, 35: 1725−1734.

[44] ŠLAPÁKOVÁ M, ZIMINA M, ZAUNSCHIRM S, KASTNER J, BAJER J, CIESLAR M. 3D analysis of macrosegregation in twin-roll cast AA3003 alloy [J]. Materials Characterization, 2016, 118: 44−49.

[45] VAN DALEN M E, SEIDMAN D N, DUNAND D C. Creep- and coarsening properties of Al−0.06at.%Sc−0.06at.%Ti at 300−450 °C [J]. Acta Materialia, 2008, 56: 4369−4377.

[46] DU Yong, CHANG Y A, HUANG Bai-yun, GONG Wei-ping, JIN Zhan-peng, XU Hong-hui, YUAN Zhao-hui, LIU Yong, HE Yue-hui, XIE Fan-you. Diffusion coefficients of some solutes in fcc and liquid Al: Critical evaluation and correlation [J]. Materials Science & Engineering A, 2003, 363: 140−151.

[47] FROST H J, ASHBY M F. Deformation-mechanism maps [M]. Oxford: Pergamon Press, 1982.

[48] ARDELL A J. Precipitation hardening [J]. Metallurgical Transactions A, 1985, 16: 2131−2165.

[49] SONG Min. Modeling the hardness and yield strength evolutions of aluminum alloy with rod/needle-shaped precipitates [J]. Materials Science and Engineering A, 2007, 443: 172−177.

[50] WANG X, EMBURY J D, POOLE W J, ESMAEILI S, LLOYD D J. Precipitation strengthening of the aluminum alloy AA6111 [J]. Metallurgical and Materials Transactions A, 2003, 34: 2913−2924.

[51] DU Qiang, TANG Kai, MARIOARA C D, ANDERSEN S J, HOLMEDAL B, HOLMESTAD R. Modeling over-ageing in Al−Mg−Si alloys by a multi-phase CALPHAD-coupled Kampmann-Wagner Numerical model [J]. Acta Materialia, 2017, 122: 178−186.

[52] KELLY P M. The effect of particle shape on dispersion hardening [J]. Scripta Metallurgica, 1972, 6: 647−656.

高强高塑性空冷 Al−Mg−Si 合金的非均质化组织构建

高一涵[1]，张欣欣[2]，周晶哲[3]，徐 鹏[1]，辛志杰[4]，高俊华[4]，时彦浩[4]，吕 由[2]，赵宇芳[4]，李京阳[1]

1. 中北大学 航空宇航学院，太原 030051；
2. 华中科技大学 化学与化工学院 先进能源材料化学教育部重点实验室，
材料化学与服役失效湖北省重点实验室，武汉 430074;
3. 广东齐力澳美高新材料股份有限公司 轻金属研究院，佛山 528137；
4. 中北大学 机械工程学院，太原 030051

摘 要：提出一种利用非均匀分布的 α-Al(Fe,Mn)Si 弥散相与 β''析出相协同提升空冷 6082 铝合金强度与塑性的方法。扫描电子显微镜(SEM)与透射电子显微镜(TEM)分析显示，不进行均匀化即可引发上述显微组织非均匀性，合金由局部的无弥散相区(DFZs)与弥散相区(DZs)以及双峰分布的 β''析出相构成。进一步的强化模型计算显示，这种非均匀的显微组织布局事实上在目标合金中构建了“软−硬”区，从而引起力学性能的改善。

关键词：Al−Mg−Si 合金；显微组织异质性；弥散相；纳米析出相；力学性能

(Edited by Bing YANG)